From Sphere to Multipod: Thermally Induced Transitions of CdSe Nanocrystals Studied by Molecular Dynamics Simulations

Zhaochuan Fan,[†] Anil O. Yalcin,[‡] Frans D. Tichelaar,[‡] Henny W. Zandbergen,[‡] Elise Talgorn,[§] Arjan J. Houtepen,[§] Thijs J. H. Vlugt,[†] and Marijn A. van Huis*[,‖]

[†]Process and Energy Laboratory, Delft University of Technology, Leeghwaterstraat 44, 2628 CA Delft, The Netherlands
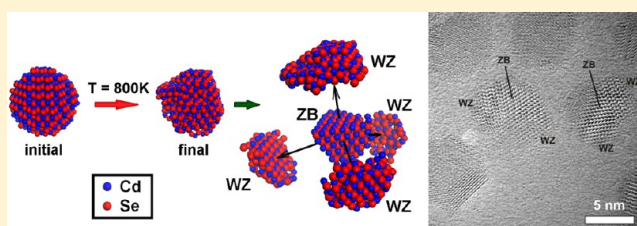
[‡]Kavli Institute of Nanoscience, Delft University of Technology, Lorentzweg 1, 2628 CJ Delft, The Netherlands

[§]Department of Chemical Engineering, Delft University of Technology, Julianalaan 136, 2628 BL Delft, The Netherlands

[‖]Soft Condensed Matter, Debye Institute for Nanomaterials Science, Utrecht University, Princetonplein 5, 3584 CC Utrecht, The Netherlands

S *Supporting Information*

ABSTRACT: Molecular dynamics (MD) simulations are used to show that a spherical zinc blende (ZB) nanocrystal (NC) can transform into a tetrapod or an octapod as a result of heating, by a local zincblende-to-wurtzite phase transformation taking place in the NC. The partial sphere-to-tetrapod or sphere-to-octapod transition occurs within simulation times of 30 ns and depends on both temperature and NC size. Surprisingly, the wurtzite (WZ) subdomains are not formed through a slip mechanism but are mediated by the formation

of highly mobile Cd vacancies on the ZB{111} Cd atomic planes. The total potential energy of a tetrapod is found to be lower than that of a ZB sphere at the same numbers of atoms. The simulation results are in good agreement with experimental high-resolution transmission electron microscopy (HR-TEM) data obtained on heated colloidal CdSe NCs.

INTRODUCTION

Cadmium selenide (CdSe) is a II−VI group semiconductor which has been widely studied.[1] There are three known structures of CdSe: wurtzite (WZ), zinc blende (ZB), and high-pressure rock salt (RS). Theoretical studies[2] showed that the WZ and ZB CdSe bulk materials have very similar energies at zero temperature and zero pressure, and in practice both WZ and ZB bulk CdSe are stable at relatively low temperatures.[3] CdSe nanocrystals (NCs) are studied extensively as a model system, as they show tunable optical and electronic properties depending on their size.[4,5] Therefore, the size-, shape-, and structure-controlled synthesis of the CdSe nanocrystals has become an important research area.[6−9] Special attention has been paid to heterostructural nanocrystals[10] (HSNCs) such as branched nanocrystals,[11−20] due to their novel and complex morphologies and the potential application in optoelectronic devices. In 2003, Manna et al.[11] reported the synthesis of CdTe nanocrystals with a tetrapod shape. Since this discovery, several other types of nanotetrapods consisting of different compounds and using various synthesis methods have been reported.[12−15] II−VI and IV−VI semiconductor nanocrystals having an octapod morphology have also been reported recently.[16−20] These multipod morphologies contain a ZB tetrahedral or octahedral core, and the WZ legs are grown on the surfaces of the ZB cores along the ± ⟨0001⟩ direction.

The crystal and electronic structure as well as mechanical, thermodynamic, and vibrational properties of bulk CdSe have

been systematically studied by means of density functional theory (DFT) calculations.[2,21−23] Wang et al.[24] have studied the geometries and electronic structure of CdSe surfaces using the tight-binding method. The passivation of CdSe surfaces by ligands and the binding energies of ligands were calculated by DFT[25] and molecular simulations,[26] respectively. In addition, much research has been conducted on the pressure-induced WZ-to-RS phase transition.[27−31] One of the most important studies was done by Grünwald et al.[27] who successfully simulated the WZ-to-RS phase transition in CdSe NCs using molecular dynamics (MD) simulations with a classical forcefield for CdSe first developed by Rabani.[32] The mechanism of this pressure-induced phase transition is somewhat controversial as the metastable intermediate *h*-MgO phase found in the MD simulations has not been observed experimentally. In contrast to the pressure-induced transformations, little is known on the effect of temperature on CdSe nanostructures.

In this work, we used MD simulations to predict a thermally induced sphere-to-multipod morphological transition in CdSe NCs mediated by local ZB-to-WZ phase transformations. The MD simulations show that an uncapped spherical CdSe NC with ZB structure transforms to a nanotetrapod or a nanooctapod upon heating. Below we will compare our results with in situ heating experiments performed in the high-

resolution transmission electron microscope (HR-TEM), whereby similar nanotetrapods were observed. The MD simulations reveal the vacancy-assisted mechanism of the WZ-to-ZB transition and indicate that the final morphology is temperature- and size-dependent.

METHODS

MD Simulations. To study the morphological and structural transformations of CdSe NCs, the empirical pair potential of CdSe developed by Rabani[32] was used to describe the interactions between atoms. The pair potential consists of two parts: Coulombic interactions and a short-ranged Lennard–Jones potential. We chose Rabani's potential because of its simplicity and effectiveness, which was demonstrated by several simulation studies[16,27,28,30,31,33] on CdSe materials. We further investigated the validity of the interaction potential at high temperatures and the capability of the interaction potential to describe surface properties. The lattice parameters of bulk CdSe for both the WZ and the ZB phases were calculated for temperatures ranging from 300 to 1000 K by MD simulations. We have also calculated the surface energies for selected WZ and ZB surfaces by lattice static (LS) simulations. Details of these calculations and the results are presented in the Supporting Information. The results show that, except for the overestimation of the thermal expansion coefficient,[34] Rabani's potential leads to quite accurate predictions for the lattice parameters of the CdSe bulk materials at high temperatures. The differences between MD simulations and X-ray diffraction experiments[34] are less than 4%. Also, the surface energies calculated by the LS simulation are in good agreement with DFT results.

Three ZB CdSe nanosphere models were constructed with radii of 1.8, 2.3, and 2.8 nm containing 880, 1720, and 3028 atoms, respectively. A WZ CdSe nanosphere (radius 1.8 nm, 882 atoms) was also constructed. All nanosphere models are isolated in vacuum without surfactants. In the MD simulations of CdSe NCs, the equations of motion were integrated using the velocity Verlet algorithm with a time step of 1 fs. During the equilibration, the velocities were rescaled to the desired temperatures. After equilibration, the temperatures were controlled by the Nose-Hoover thermostat.[35] The CdSe nanosphere models were constructed by cutting a sphere from a bulk CdSe crystal. As we study isolated NCs in vacuum, no periodic boundaries were applied. The electrostatic interactions were calculated by taking into account all atom pairs, and the short-ranged Lennard–Jones interaction was truncated and shifted at 10 Å. MD simulations of 30 ns were performed for all systems, out of which the first 3 ns were used to equilibrate configurations.

Synthesis of CdSe Nanocrystals. Following an adapted recipe of Mekis et al.,[36] two precursors were prepared in a N_2 purged glovebox by dissolving 0.474 g of Se (325 mesh) in 6 mL of TOP (trioctylphosphine) and 0.36 g of Cd(Ac)$_2$ in 9 mL of TOP, respectively. Subsequently, the following synthesis was done in a Schlenk line to provide oxygen- and water-free conditions. Specifically, 24 g of TOPO (trioctylphosphine oxide) was heated to 180 °C in vacuum under periodic flushing with N_2. After cooling down to 100 °C, 15 g of HDA (1-hexadecylamine) and 0.45 g of TDPA (1-tetradecylphosphonic acid) were added and dried at 120 °C in vacuum during 30 min under periodic flushing with N_2. The TOP-Se precursor was injected, and the solution was heated to 300 °C under N_2 flow. Under vigorous stirring, the TOP-Cd(Ac)$_2$ precursor was injected to induce nucleation of CdSe nanoparticles. During the growth at 280 °C aliquots were taken to monitor the growth rate. After 550 s the reaction was stopped by cooling down the remaining reaction volume to room temperature. At 55 °C 30 mL of toluene was injected to avoid solidification of the TOPO. The obtained dispersion was purified by repeated washing with MeOH and precipitation of particles in a centrifuge at 3000 rpm for 5 min. The final stock of particles was dispersed in chloroform.

TEM In Situ Heating Experiments. Heating experiments were conducted in situ in the transmission electron microscope (TEM) on CdSe NCs with a diameter of about 6 nm. The NCs were dropcast

onto MEMS microheaters with SiN electron-transparent viewing windows, which enables atomic-resolution imaging while heating inside the TEM.[37] A Cs-aberration-corrected cubed Titan TEM was used operating at 300 kV.

RESULTS AND DISCUSSION

Sphere-to-Tetrapod Transformation. Figure 1a and Supporting Movie M1 show the time evolution of ZB spherical
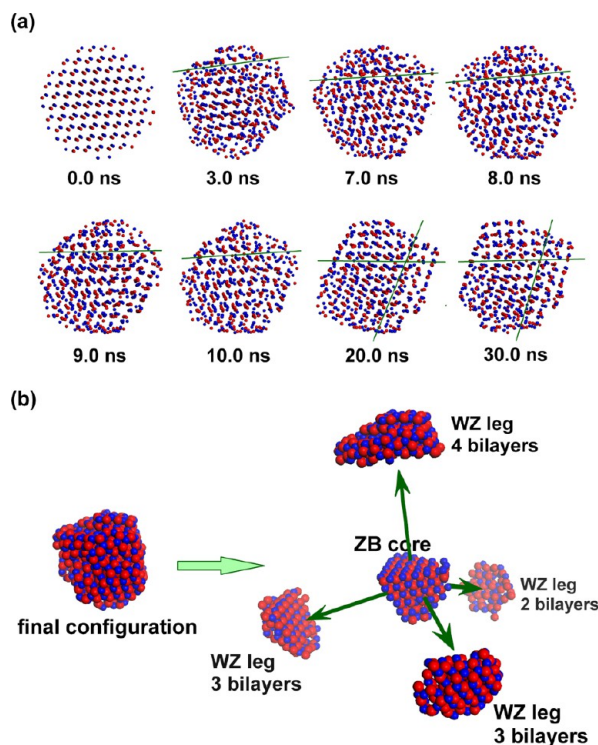

Figure 1. (a) Snapshots of Cd$_{440}$Se$_{440}$ NCs from MD simulations at 800 K. Surface atoms show structural rearrangements after 3 ns. From 7 to 9 ns, a local ZB-to-WZ transition takes place on the third outermost bilayer. The green line on the snapshot at 3 ns indicates a boundary betweeen the second and the third outermost ZB{111}/WZ{0001} bilayer; the green lines on the snapshots at 7, 8, 9, and 10 ns indicate the boundaries between the third and the fourth outermost bilayers; the green lines on the snapshots at 20 and 30 ns indicate the boundaries between the WZ and ZB domain. (b) Deconstruction of the final configuration (a tetrapod morphology with one ZB core and four short WZ legs). In all snapshots, the blue and red spheres are Cd and Se atoms, respectively.

Cd$_{440}$Se$_{440}$ NC at 800 K during 30 ns. Surface reconstruction takes place at the start of the simulation: the surface becomes angular and rugged. Despite the thermal motion of the atoms, it is still possible to investigate the local crystalline order. The first two outermost bilayers transform from the ZB structure to the WZ structure in 3 ns. Here, we define a bilayer as a {CdSe} pair of nearest WZ {0001} planes or a {CdSe} pair of nearest ZB {111} planes. From 7 to 10 ns, the ZB-to-WZ transition also takes place in the third outermost bilayer (Figure 1a) of the NC. No clear local structural transition is then observed until the end of the MD simulation. After 20 ns, the Cd$_{440}$Se$_{440}$ NC reaches a relatively stable configuration. During the 30 ns MD simulation, the structure of the NC transforms from purely ZB to heterostructural whereby the interface between the ZB and WZ domains is along the WZ{0001}/ZB{111} atomic planes.
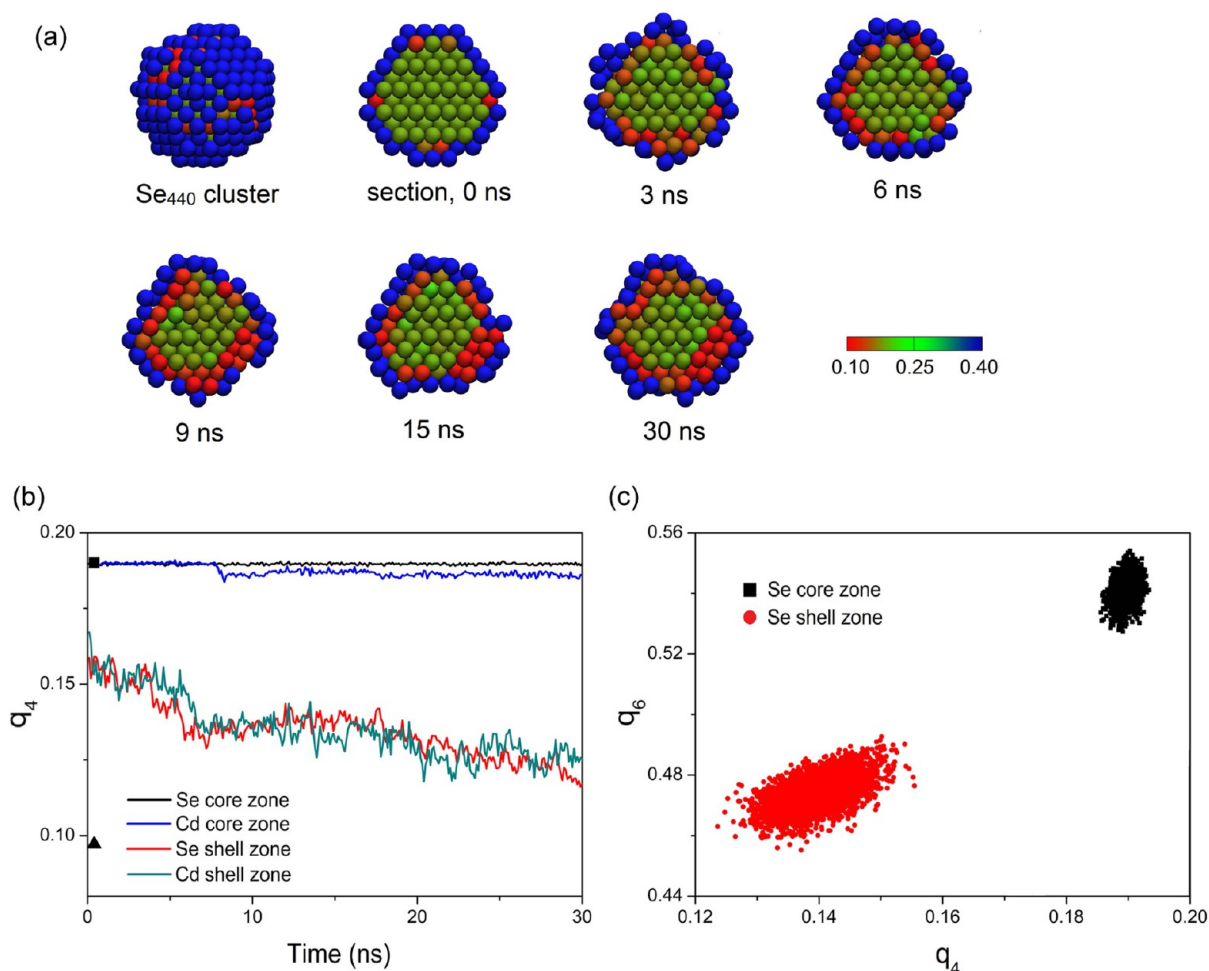
Figure 2. (a) Snapshots of the Se_{440} sublattice colored by the value of the bond order parameter q_4 at 800 K. The surface atoms (see the definition in the main text) are given a value of 0.4 in order to not take them into account. (b) Plots of the averaged q_4 for all the Se or Cd atoms in one zone (see the definitions of the "core zone" and "shell zone" in the main text) as a function of time, fluctuating due to thermal vibrations. The black square and the black triangle indicate the referenced ideal values of q_4 of the fcc and hcp Se sublattice in the CdSe bulk materials at 800 K, respectively, where $q_{4-fcc} = 0.190$ and $q_{4-hcp} = 0.097$ at 800 K. (c) The q_4–q_6-plane for the Se_{440} cluster in the "core zone" and the "shell zone". Each point corresponds to the averaged values of q_4 and q_6 for all of the atoms in different zones, calculated at a single time.

To visualize the transition, different parts of the tetrapod are shown separately in Figure 1b: the WZ domains are displayed separately from the ZB core toward the <0001> direction. The heated ZB $Cd_{440}Se_{440}$ NC exhibits a distinct tetrapod morphology with a ZB core and four short WZ legs. The lengths of the four WZ legs differ: the longest one contains four bilayers, and the shortest one contains only two. We always count the bilayer at the boundary of the ZB and the WZ domains as in the WZ structure. The ZB core has a tetrahedral morphology, and the four WZ legs are connected onto the four ZB Cd-terminated {111} facets of the tetrahedral core.

Before elaborating on the structural details of the nano-tetrapod, we first mention the simulation result for the spherical *wurtzite* $Cd_{441}Se_{441}$ NC, which leads to very different results. A local structural transition from the WZ structure to a body-centered-tetragonal structure (BCT) is observed. This transition was also found and studied in previous molecular simulations and DFT calculations for CdSe and other II–VI semiconductor nanostructures and bulk materials,[38−42] and recently it was observed directly in ZnO nanoislands by aberration-corrected TEM.[43] During the simulation, the morphology of the WZ $Cd_{441}Se_{441}$ NC changes from spherical

to rod-like, as shown in Figure S2 of the Supporting Information.

The structural transition of the *zinc blende* NC can be quantified by local bond order parameters.[44] Local bond order parameters preserve the information of the local structure by symmetry analysis and are commonly used to distinguish among different crystal structures and the liquid phase.[45−47] Detailed information about the definition of the local bond order parameters is presented in the Supporting Information. Here, the order parameter q_4 is chosen to monitor the structural evolution, and the q_4–q_6 plane is used to distinguish the ZB and the WZ structures. Either all Cd atoms or all Se atoms are removed from the $Cd_{440}Se_{440}$ NC, so that cationic and anionic sublattices are obtained. Both sublattices are face-centered cubic (fcc) in the ZB phase and hexagonal close packed (hcp) in the WZ phase. Atoms at the surfaces are considered separately from the atoms inside the NC, as the local structure of surface atoms cannot be evaluated precisely by bond order parameters based on nearest neighbor analysis. The surface atoms are distinguished by counting the numbers of the nearest neighbors for each atom in the Cd or Se sublattices; an atom is defined as a surface atom if the number of nearest neighbors is less than 9, and the atoms are defined to be nearest
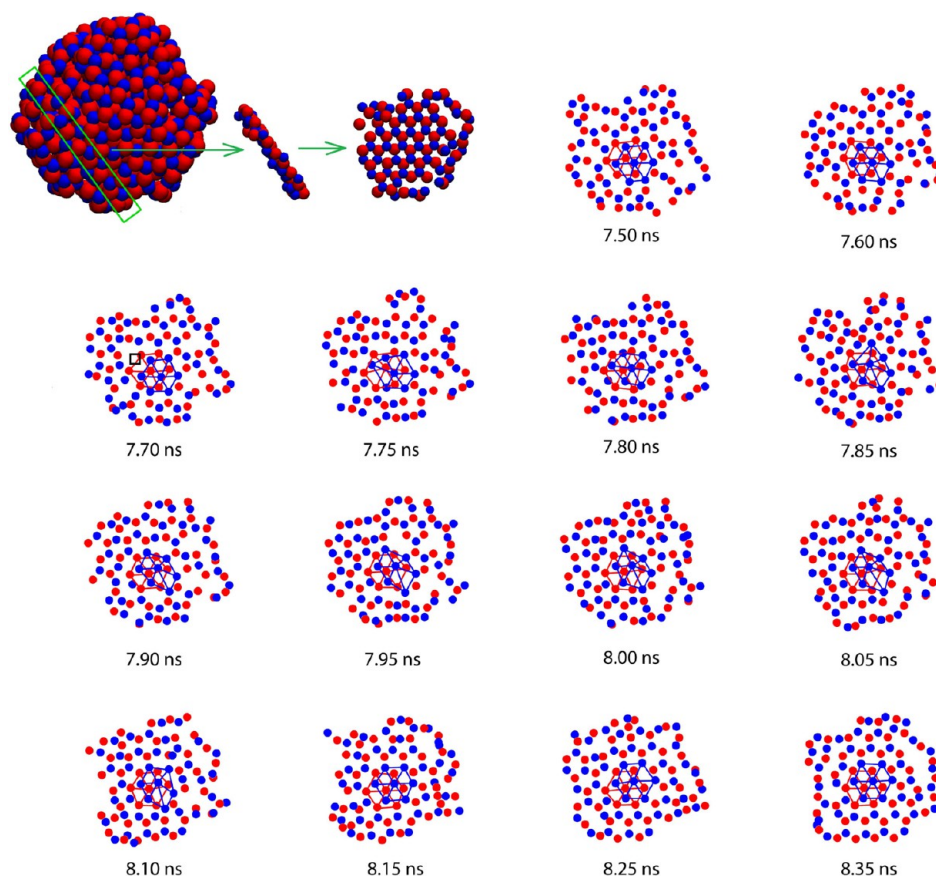
Figure 3. Snapshots of one of the third outermost ZB (111) (or WZ(0001)) bilayers from 7.50 to 8.35 ns. The shapshot on the upper left indicates where the bilayer is located in the NC and how it is oriented. Seven Cd and seven Se atoms in the middle of the bilayer are connected with lines to show the deformation of lattice sites during the local structural transition. The black square in the 7.70 ns snapshot indicates one of the Cd vacancies which cause local distortions and assist the ZB-to-WZ local structural transition. The blue and red spheres (dots) are Cd and Se atoms, respectively. Sometimes strings of atoms seem to appear, for example at the right-hand side of the 8.05 and 8.35 ns snapshots. This feature is caused by the presence of a string of vacancies.

neighbors if their interatomic distance is less than 5.4 Å. We define a "core zone" consisting of all atoms within 0.8 nm of the center of the NC and a "shell zone" consisting of all atoms outside a sphere with a radius of 1.1 nm. Using this division, the atoms in the ZB core and in the WZ legs can be distinguished effectively. The atoms at the ZB/WZ boundaries are thereby not included in our analysis. As a reference, we first calculated the averaged values of q_4 for fcc and hcp structures in CdSe bulk materials at 800 K. $q_{4-fcc} = 0.190$ and $q_{4-hcp} = 0.097$ at 800 K. The values of the order parameters q_4 and q_6 in the Se_{440} and Cd_{440} sublattices were calculated as a function of time. A fixed value of $q_4 = 0.4$ was allocated to surface atoms. In Figure 2a, simulation snapshots of the Se sublattice colored by q_4 show the structural evolution of the NC. At 0 ns, the color of most of the atoms, except for the surface atoms, are green corresponding to $q_4 \approx 0.2$, which indicates an initial fcc structure of the sublattice. During the MD simulation, more and more atoms on the edge turn to red corresponding to a decrease of q_4 to 0.13. After 9 ns, two layers of red atoms on the lower right part of the Se sublattice section are observed, coinciding with the longest WZ leg that has four WZ bilayers. In Figure 2b, the averaged q_4 with respect to all the same atoms (either Cd or Se) at a certain zone (either the "core zone" or the "shell zone") are plotted as a function of time. The plots of the averaged values of q_4 for Cd and Se atoms in the same zone are overlapping, as the structures of Cd and Se sublattice are

approximately identical. The result (Figure 2b) shows that the averaged q_4 of the atoms in the core zone remains nearly constant, coinciding with the fcc structure. This clearly shows that the atoms in the core zone remain in the ZB structure during the simulations. The averaged q_4 of the atoms in the shell zone decreases from 0.165 to 0.125 with relatively large fluctuations, suggesting a ZB-to-WZ structural transition. The q_4–q_6-plane for the Se_{440} sublattice in the core and shell zones are shown in Figure 2c. Each data point corresponds to q_4 averaged over all atoms in one zone at a given time step in the last 15 ns. The fcc structure in the ZB core zone and the hcp structure in the WZ shell zone can thus easily be distinguished.

Atomic-Scale Transition Mechanism. The question now arises: what is the underlying mechanism of the morphological and local structural transitions? From a close inspection of the results, it is clear that the ZB-to-WZ local structural transition starts from the outermost layer and then proceeds into the inner layers. In our simulation, the first two outermost ZB {111} bilayers change quickly (within 3 ns) into WZ {0001} bilayers, and the transition of the third outermost bilayer starts after approximately 7.5 ns. The snapshots of the third outermost bilayer around the transition provide the essential information (Figure 3): Until 7.60 ns, the Cd and Se atoms in the bilayer are located at the ZB lattice sites, but deformations can be identified at the edge of the plane. From 7.70 ns onward, several Cd atoms in the central area migrate to the WZ sites

assisted by Cd vacancies. After 8.15 ns, the whole Cd layer is shifted from the ZB sites to the WZ sites. It is important to note that the slip (the mutual displacement along a so-called slip plane of the two parts of the structure at either sides of the slip plane) of the Cd layer is very gradual, taking place through a large number of individual atomic jumps, and is greatly assisted by point defects (Cd vacancies). In general, vacancies can be annealed out more easily in a nanocrystal than in a bulk material, since a defect needs to travel a much shorter distance to reach the surface. On the other hand, the surface also acts as a source of vacancies so that defects are easily produced at elevated temperatures. Elevated temperatures also enhance the mobility of the defects, thereby accelerating the process of the ZB-to-WZ transition.

The difference in potential energies between the bulk WZ and bulk ZB CdSe at 0 K is very small: DFT calculations[2] indicate an energy difference of just 2 meV per {CdSe} pair. The potential energies of the nanocrystals are strongly dependent on the morphology. It is difficult to compare the potential energies of the tetrapod with a ZB sphere at 800 K, since a spherical morphology is structurally unstable in the ZB structure at 800 K. However, potential energies can be compared at a lower temperature (200 K), whereby the ZB sphere is metastable. MD simulations of the initial spherical ZB NC were performed at a temperature of 200 K in 20 ns, whereby the first 4 ns were used to equilibrate the system. At such a low temperature, the configuration retains both a spherical morphology and the ZB structure. Next, the configuration of the heated tetrapod obtained from the MD simulation at 800 K was cooled down to 200 K in three steps. At each step the temperature was reduced by 200 K, and the system was equilibrated for 5 ns. At $T = 200$ K, an extended MD simulation of 4 ns was performed. It turns out that the final configuration of the NC at 200 K retains the tetrapod-like shape. The averaged potential energy in the last 4 ns of the tetrapod is 40 meV per {CdSe} pair less than the ZB sphere at 200 K. We therefore conclude that the tetrapod configuration is energetically preferred over the spherical ZB NC configuration.

Surfaces always play an important role in nanocrystals due to the large surface-to-volume ratio. As mentioned previously, the Rabani CdSe potential describes the surface properties of CdSe materials relatively well. The results of the LS simulations in this work indicate that CdSe WZ $\{11\bar{2}0\}$ and $\{10\bar{1}0\}$ and ZB $\{110\}$ are the most stable facets with only little differences in surface energy (less than 0.02 J/m^2). The polar surfaces, WZ $\{0001\}$ and $\{000\bar{1}\}$ and ZB $\{111\}$ and $\{\overline{111}\}$ facets, are relatively unstable; that is, surface energies of these facets are relatively high. The most unstable surfaces are the ZB Cd-terminated $\{001\}$ and Se-terminated $\{00\bar{1}\}$ facets. DFT calculations[25] showed that ligands such as methyl phosphoric acid (MPA), methyl amine (MA), or trioctylphosphine oxide (TOPO) can greatly reduce the surface energies of the unstable surfaces on the CdSe NCs. For example, the surface energy of the WZ Cd-terminated (0001) facet passivated by MPA or MA can be reduced from 80 meV/Å^2 (bare surface) to approximately 40 meV/Å^2 (capped surface) which is comparable to the surface energies of the most stable WZ $\{11\bar{2}0\}$ or $\{10\bar{1}0\}$ facets passivated by the same kind of ligand. Using proper ligands, NCs can be synthesized with surfaces that without ligands would be unstable.[48] Evaporating the ligands by heating also activates the unstable surfaces again and causes structural or morphological transitions. Using MD simulations, Schapotschnikow et al.[49] showed that after evaporation of the

ligands by annealing, a nearly spherical PbSe NC capped by ethylamine surfactants will undergo a morphological transition from multifaceted to cubic at 450 K. Similarly, the morphological and local structural transitions of the ZB CdSe NC in our simulation could be the consequence of exposing its unstable surfaces to vacuum.

Experimental HR-TEM Results. Strong correspondence was found between the simulation results and the results of the annealing experiments conducted in situ in the TEM on 6-nm-diameter CdSe NCs. The results are displayed in Figure 4. Directly after dropcasting, deposits of the solution and ligands prevent high-resolution imaging. Shortly after low-temperature
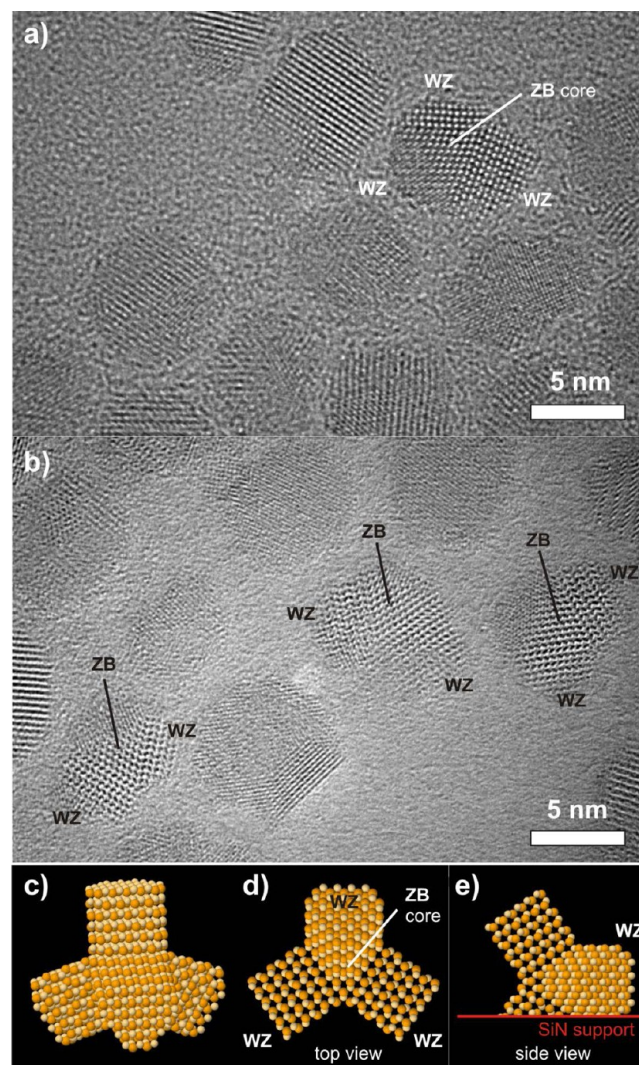

Figure 4. (a) HRTEM image of CdSe nanocrystals after low temperature annealing (350 K). The HR fringes reveal that the NCs consist of multiple domains, some of which are ZB and some of which are WZ. One particular NC has a nearly spherical shape, but also contains all of the elements of a tetrapod (the ZB core and the WZ pods are indicated). (b) After annealing to a temperature of 390 K, several NCs evolve into tetrapods, whereby the WZ legs become more pronounced. (c) Schematic of a tetrapod in a perspective view. (d) Schematic showing the projection of the tetrapods observed in the HRTEM images. (e) Schematic showing side view of d: two pods are lying onto the support, the third pod is pointing away from the support, while the fourth (short) pod is pointing into the support; the latter two are overlapping in projection.

annealing at a temperature of 350 K, the high-resolution fringes reveal that the spherical NCs consist of multiple domains, which can be either WZ or ZB. Here, we remark that in the HRTEM images displayed in the reference work for the synthesis,[36] also multiple domains can be distinguished. One spherical NC in Figure 4a displays already at this stage a precursor state for transforming into tetrapods: while this NC is nearly spherical, it displays already a ZB core and short WZ legs and is very similar to the simulation result obtained after 30.0 ns shown in Figure 1. Upon continued annealing for approximately 20 min at a temperature of 390 K, several NCs transform into tetrapods with more elongated WZ pods, as shown in panel b of Figure 4. The schematics in panels (d,e) show the orientation of the tetrapods observed in the experiments, whereby in general two of the pods are lying flat onto the SiN membrane support. Not all spherical NCs transformed into tetrapods: some evolved into single crystals (WZ or ZB), while others formed tripods, bipods, or dimers. Supporting Movie M2 shows an isolated bipod or tripod at an elevated temperature of 400 K, which was followed in time during 3 min. Small changes are observed in the arrangement of atomic planes (width, occupancy) and in the overall morphology. These changes may be caused not only by the elevated temperature but may be additionally induced by the electron beam. However, the multipod structures shown in Figure 4 were found everywhere on the SiN support membrane, also in areas that were not previously exposed to the electron beam. Because of nonideal orientations of the heterogeneous nanocrystals with respect to the projection plane, the morphology of many NCs could not be distinguished. The synthesis and temperature treatment could be fine-tuned to yield a higher fraction of tetrapods after annealing, which is beyond the scope of the present work. A more extensive experimental study will be published elsewhere.

A direct comparison between the simulation results and experimental studies is difficult, as in the experimental situation the initial NCs are covered by stabilizing surfactants, which has a profound effect on the surface chemistry and therefore on the overall stability of the NCs. The extension of the WZ pods during annealing was not observed in the simulations, but this is most likely due to the limited simulation times (30 ns in simulation versus ~20 min in experiment). Other major differences between experiment and theory are the presence of a support in the experiments that is absent in the simulations and a different starting configuration (WZ/ZB distribution within the NCs). Nonetheless, the preliminary experiments show that the tiny tetrapods found in the simulations can actually be formed and do have a certain thermal stability. The merit of the simulations is that they provide fundamental insight into the ZB-WZ transition at the atomic scale: whereas a slip mechanism would be in the line of expectation, here we show that slip does not occur, and that instead the transformation is mediated by mobile vacancies on the cation sublattice.

Temperature and Size Effects. As already mentioned, the time scale in the experiments is many orders of magnitude larger than in the MD simulations. Therefore, in our simulations the temperatures were artificially elevated in order to shorten the transition times. For instance, CdSe NCs melt at a temperature above 750 K in the TEM, but in our MD simulations of 30 ns, we did not observe melting below 1000 K. A similar situation was also present in the study of the pressure induced WZ-to-RS transition in CdSe nanocrystals by

Grünwald et al.[27] It should be noted that the interaction potentials used in this work were developed by fitting the bulk properties of CdSe, so the different energetics and changes of the electronic structure of nanosized CdSe are not accounted for. Therefore, the temperatures in the simulations should be compared with the temperatures in the experiments in a qualitative manner. Figure 5 shows a graphical overview of
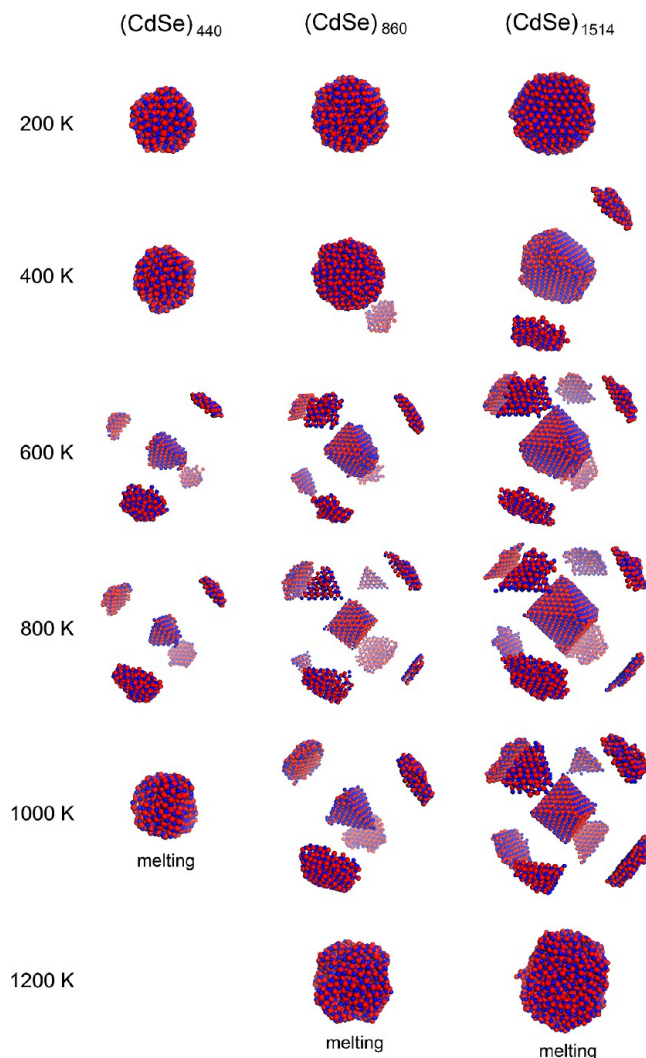

Figure 5. Final configurations of CdSe NCs with different sizes at various temperatures. When the ZB-to-WZ local structural transition takes place, for clarity the WZ domains are shifted along the <0001> directions. The blue and red spheres are cadmium and selenium, respectively.

configurations obtained at six different simulated temperatures, for three different NC sizes. The following striking features are observed: (1) Below 400 K, no apparent sphere-to-multipod transition is found within 30 ns. The spherical ZB CdSe NCs only show some rearrangement of surface atoms. (2) At temperatures of 400−1000 K, the sphere-to-multipod transitions are observed. Identical NCs evolve into configuration with longer legs within 30 ns when heated to higher temperatures. (3) In a temperature range of 1000−1200 K, melting of the NCs is observed.

Another interesting question is whether instead of a tetrapod, an octapod could be formed by heating. In the case of an octapod, the ZB core is octahedral with four equivalent {111}

facets as well as four equivalent $\{\overline{1}11\}$ facets. However, it is generally known that a II–VI semiconductor nanooctapod is more difficult to be synthesize than a nanotetrapod, because the four ZB $\{\overline{1}11\}$ facets are more reactive than the four ZB $\{111\}$ facets during colloidal synthesis of nanomaterials.[20] Only using a proper ZB core (a seed) with octahedral morphology, proper ligands, and well-controlled reaction temperatures, can these nanooctapods be synthesized successfully. Nonetheless, CdSe NCs with octapod morphology are observed in some cases in our simulations. As shown in Figure 5, final configurations with a octapod morphology are observed for the $Cd_{860}Se_{860}$ at 800 K and $Cd_{1514}Se_{1514}$ NC at 800 and 1000 K. In this work, the octapod-like morphology is only found in the largest NC model. This is in good agreement with experimental synthesis reports of nanotetrapods and nanooctapods. For octapods, it is required that the eight ZB$\{111\}$ facets of the core are well developed, which can be only achieved if the ZB core (seed) is sufficiently large. In addition, it is notable that the final configuration of the $Cd_{1514}Se_{1514}$ NC at 600, 800, and 1000 K shows octapod-like morphologies, while the $Cd_{860}Se_{860}$ NC displays an octapod morphology at 600 and 800 K, but at a higher temperature of 1000 K a tetrapod is formed. This unexpected result is in line with experimental results. In the synthesis of branched NCs, the reaction temperature is a critical factor to determine the morphologies of the products. Deka et al.[20] pointed out that in the synthesis of CdSe branched NCs, CdSe nanooctapods were observed in the temperature range between 593 and 623 K, and the final products would be nanotetrapods instead if the reaction temperature was elevated to 653 K.

CONCLUSIONS

In summary, the morphological and structural transformations of the ZB CdSe NCs at high temperatures were studied using MD simulations with the Rabani CdSe potential. In the temperature range 600–1000 K, ZB CdSe nanospheres with different sizes change into heterogeneous NCs with tetrapod- or octapod-like morphologies. The morphology of the final configurations in the MD simulations depends on the size of the NCs and the temperature. The nanotetrapod consists of one tetrahedral ZB core and four WZ legs. The $\{111\}$ surfaces on the ZB core connect with the $\{0001\}$ surfaces of the WZ legs. In contrast to the tetrapod, octapods have ZB cores in an octahedral shape, whose four $\{111\}$ and four $\{\overline{1}11\}$ facets can adjoin with eight WZ legs. By means of MD simulations we have mimicked possible annealing experiments of the CdSe NCs in vacuum, and technically, the result can be clarified by characterizations such as HR-TEM or high-temperature X-ray diffraction, assuming ligands do not play any role (bare surfaces). A close inspection shows that the local ZB-to-WZ transition is caused by the shift of the Cd layer within the ZB $\{111\}$ atomic plane, which is enabled by a high mobility of individual Cd vacancies. This finding is also of importance for understanding the process of cation exchange,[50,51] whereby cations within the nanostructure are (partly) replaced with other cations (e.g., Pb ions in PbSe nanorods are partly exchanged with Cd ions so that core/shell PbSe/CdSe nanorods are obtained). It is commonly observed that the overall morphology of the nanostructures remains intact, presumably because the anion (Se) sublattice does not participate in the cation exchange process. This is in line with the current finding of high atomic mobility on the cation sublattice. The total potential energy of a tetrapod morphology

was found to be *lower* than that of a spherical ZB NC having the same number of atoms. The ZB or WZ CdSe NCs that are synthesized in experiments contain unstable surfaces with relatively high surface energies, but these unstable surfaces are passivated by ligands. We suggest that if these ligands could be entirely removed, for example by evaporation, a new morphology or structure with a lower potential energy will eventually be found. The simulation results are in good agreement with experimental results obtained by in situ heating of 6 nm sized CdSe NCs inside the transmission electron microscope. The heterogeneous transition of the CdSe NCs could emerge as a new method of fabricating tetrapod or octapod morphologies and will be subject of future investigations.

ASSOCIATED CONTENT

Ⓢ Supporting Information

MD simulations of the temperature-dependent lattice parameters of WZ and ZB bulk CdSe, LS simulations of CdSe low-index surface energies, details of MD simulation settings, results of MD simulations for a WZ spherical CdSe NC, a brief description of local bond order parameters, experimental synthesis details of CdSe NCs, and two Supporting Movies (M1 and M2). This material is available free of charge via the Internet at http://pubs.acs.org.

AUTHOR INFORMATION

Corresponding Author
m.a.vanhuis@uu.nl

Notes
The authors declare no competing financial interest.

REFERENCES

(1) Sadao, A. *Properties of Group-IV, III-V and II-VI Semiconductors*; Wiley: New York, 2005.
(2) Wei, S.-H.; Zhang, S. B. *Phys. Rev. B* **2000**, *62*, 6944–6947.
(3) Lawrence, M. F.; Du, N.; Philippe, R.; Dodelet, J.-P. *J. Cryst. Growth* **1987**, *84*, 133–144.
(4) Katz, D.; Wizansky, T.; Millo, O.; Rothenberg, E.; Mokari, T.; Banin, U. *Phys. Rev. Lett.* **2002**, *89*, 086801.
(5) de Mello Donegá, C.; Bode, M.; Meijerink, A. *Phys. Rev. B* **2006**, *74*, 085320.
(6) Peng, X.; Manna, L.; Yang, W.; Wickham, J.; Scher, E. C.; Kadavanich, A.; Alivisatos, A. P. *Nature* **2000**, *404*, 59.
(7) Shieh, F.; Saunders, A. E.; Korgel, B. A. *J. Phys. Chem. B* **2005**, *109*, 8538–8542.
(8) Kumar, S.; Nann, T. *Small* **2006**, *2*, 316–329.
(9) Manna, L.; Scher, E. C.; Alivisatos, A. P. *J. Am. Chem. Soc.* **2000**, *122*, 12700–12706.
(10) Donegá, C. d. M. *Chem. Soc. Rev.* **2011**, *40*, 1512–1546.
(11) Manna, L.; Milliron, D. J.; Meisel, A.; Scher, E. C.; Alivisatos, A. P. *Nat. Mater.* **2003**, *2*, 382–385.
(12) Milliron, D. J.; Hughes, S. M.; Cui, Y.; Manna, L.; Li, J.; Wang, L.-W.; Alivisatos, A. P. *Nature* **2004**, *430*, 190–195.

(13) Asokan, S.; Krueger, K.; Colvin, V.; Wong, M. *Small* **2007**, *3*, 1164−1169.

(14) Xu, H.; Liang, Y.; Liu, Z.; Zhang, X.; Hark, S. *Adv. Mater.* **2008**, *20*, 3294−3297.

(15) Fiore, A.; Mastria, R.; Lupo, M. G.; Lanzani, G.; Giannini, C.; Carlino, E.; Morello, G.; De Giorgi, M.; Li, Y.; Cingolani, R.; Manna, L. *J. Am. Chem. Soc.* **2009**, *131*, 2274−2282.

(16) He, X.; Gao, L. *J. Phys. Chem. C* **2009**, *113*, 10981−10989.

(17) Cao, X.; Zhao, C.; Lan, X.; Yao, D.; Shen, W. *J. Alloys Compd.* **2009**, *474*, 61−67.

(18) Bashouti, M.; Lifshitz, E. *Inorg. Chem.* **2008**, *47*, 678−682.

(19) Wang, X.; Xi, G.; Liu, Y.; Qian, Y. *Cryst. Growth Des.* **2008**, *8*, 1406−1411.

(20) Deka, S.; Miszta, K.; Dorfs, D.; Genovese, A.; Bertoni, G.; Manna, L. *Nano Lett.* **2010**, *10*, 3770−3776.

(21) Deligoz, E.; Colakoglu, K.; Ciftci, Y. *Physica B* **2006**, *373*, 124−130.

(22) Puzder, A.; Williamson, A. J.; Gygi, F.; Galli, G. *Phys. Rev. Lett.* **2004**, *92*, 217401.

(23) Tan, J.-J.; Cheng, Y.; Zhu, W.-J.; Gou, Q.-Q. *Commun. Theor. Phys.* **2008**, *50*, 220.

(24) Wang, Y. R.; Duke, C. B. *Phys. Rev. B* **1988**, *37*, 6417−6424.

(25) Manna, L.; Wang, L.; Cingolani, R.; Alivisatos, A. P. *J. Phys. Chem. B* **2005**, *109*, 6183−6192.

(26) Schapotschnikow, P.; Hommersom, B.; Vlugt, T. J. H. *J. Phys. Chem. C* **2009**, *113*, 12690−12698.

(27) Grünwald, M.; Rabani, E.; Dellago, C. *Phys. Rev. Lett.* **2006**, *96*, 255701.

(28) Zahn, D.; Grin, Y.; Leoni, S. *Phys. Rev. B* **2005**, *72*, 064110.

(29) Shimojo, F.; Kodiyalam, S.; Ebbsjö, I.; Kalia, R. K.; Nakano, A.; Vashishta, P. *Phys. Rev. B* **2004**, *70*, 184111.

(30) Ye, X.; Sun, D. Y.; Gong, X. G. *Phys. Rev. B* **2008**, *77*, 094108.

(31) Grünwald, M.; Dellago, C. *J. Chem. Phys.* **2009**, *131*, 164116.

(32) Rabani, E. *J. Chem. Phys.* **2002**, *116*, 258−262.

(33) Mandal, T. *Appl. Phys. Lett.* **2012**, *101*, 021906.

(34) Iwanaga, H.; Kunishige, A.; Takeuchi, S. *J. Mater. Sci.* **2000**, *35*, 2451−2454.

(35) Hoover, W. G. *Phys. Rev. A* **1985**, *31*, 1695−1697.

(36) Mekis, I.; Talapin, D. V.; Kornowski, A.; Haase, M.; Weller, H. *J. Phys. Chem. B* **2003**, *107*, 7454−7462.

(37) van Huis, M. A.; Young, N. P.; Pandraud, G.; Creemer, J. F.; Vanmaekelbergh, D.; Kirkland, A. I.; Zandbergen, H. W. *Adv. Mater.* **2009**, *21*, 4992−4995.

(38) Morgan, B. J.; Madden, P. A. *Phys. Chem. Chem. Phys.* **2007**, *9*, 2355−2361.

(39) Hamad, S.; Richard, C.; Catlow, A. *J. Cryst. Growth* **2006**, *294*, 2−8.

(40) Morgan, B. J. *Phys. Rev. B* **2009**, *80*, 174105.

(41) Wang, J.; Kulkarni, A. J.; Sarasamak, K.; Limpijumnong, S.; Ke, F. J.; Zhou, M. *Phys. Rev. B* **2007**, *76*, 172103.

(42) Morgan, B. J. *Phys. Rev. B* **2010**, *82*, 153408.

(43) He, M.-R.; Yu, R.; Zhu, J. *Angew. Chem.* **2012**, *124*, 7864−7867.

(44) Steinhardt, P. J.; Nelson, D. R.; Ronchetti, M. *Phys. Rev. B* **1983**, *28*, 784−805.

(45) Moroni, D.; ten Wolde, P. R.; Bolhuis, P. G. *Phys. Rev. Lett.* **2005**, *94*, 235703.

(46) Coasne, B.; Jain, S. K.; Naamar, L.; Gubbins, K. E. *Phys. Rev. B* **2007**, *76*, 085416.

(47) Auer, S.; Frenkel, D. Numerical Simulation of Crystal Nucleation in Colloids. In *Advanced Computer Simulation*; Holm, C., Kremer, K., Eds.; Springer: Berlin/Heidelberg, 2005; Vol. *173*, pp 130−130, DOI: 10.1007/b99429.

(48) Mohamed, M. B.; Tonti, D.; Al-Salman, A.; Chemseddine, A.; Chergui, M. *J. Phys. Chem. B* **2005**, *109*, 10533−10537.

(49) Schapotschnikow, P.; van Huis, M. A.; Zandbergen, H. W.; Vanmaekelbergh, D.; Vlugt, T. J. H. *Nano Lett.* **2010**, *10*, 3966−3971.

(50) Casavola, M.; van Huis, M. A.; Bals, S.; Lambert, K.; Hens, Z.; Vanmaekelbergh, D. *Chem. Mater.* **2012**, *24*, 294−302.

(51) Li, H.; Zanella, M.; Genovese, A.; Povia, M.; Falqui, A.; Giannini, C.; Manna, L. *Nano Lett.* **2011**, *11*, 4964−4970.